Systematic investigation of pseudogaps in In, Al, and Pb islands

Xuefeng Wu,[1] Chaoqiang Xu,[1] Kedong Wang,[1,2,*] and Xudong Xiao[1,3,†]

[1]*Department of Physics, The Chinese University of Hong Kong, Shatin, Hong Kong, China*

[2]*Department of Physics, South University of Science and Technology of China, Shenzhen, Guangdong 518055, P. R. China*

[3]*Center for Photovoltaics and Solar Energy, Shenzhen Institutes of Advanced Technology, Chinese Academy of Sciences, Shenzhen 518055, P. R. China*

(Received 13 May 2015; published 27 July 2015)

The novel pseudogap state has been systematically studied on flat-top In, Al, and Pb islands/films grown on Si(111) surfaces with scanning tunneling microscopy. Our observations and analysis suggest that the interplay between electron-phonon interaction and quantum confinement, the dynamic Coulomb blockade, and the orthodox Coulomb blockade are, respectively, the dominant mechanism of the formation of such pseudogap states in the flat-top metal islands at different island size scales. Our results can help to settle the dispute on the origins of the pseudogap state in such systems.

DOI: 10.1103/PhysRevB.92.035434 PACS number(s): 73.21.Fg, 72.10.Di, 73.23.Hk, 74.78.−w

I. INTRODUCTION

Recently a novel pseudogap feature near the Fermi level has been observed in nanosized structures and attracted more and more research interests [1–5]. Apart from the fact that the pseudogap state can further modify the electronic density of state (DOS) near the Fermi level, its evolution from the superconductivity gap for Pb islands shows surprising similarity to that for high temperature superconductors.

However, the origin of such a pseudogap state remains in debate. Based on the interplay between the quantum confinement and the electron-phonon scattering for electrons in a two-dimensional (2D) thin film, Wang *et al.* attributed the pseudogap or pseudopeak structure near the Fermi level to the improved interference of the elongated electron lifetime within an energy window of Debye energy [1]. This mechanism has also successfully predicted a pseudopeak structure for thin films with a quantum well state (QWS) near the Fermi level, which was observed by experiment. However it failed to explain the island size dependent pseudogap. More recently, Schackert *et al.* owe this pseudogap to phonon assisted inelastic tunneling and use it to measure the local Eliashberg function of the Pb islands [2]. In a paper by Brun *et al.* [3], a model based on dynamic Coulomb blockade (DCB) effect, which takes into account the energy exchange between the single tunneling electron through the junction and the electromagnetic environment, was proposed and could explain the island size dependence, in addition to the existence of, a gap feature. Kim *et al.* attributed the pseudogap to the combined influences of electron-electron interactions and disorder in the thin film without providing further details [4]. For the pseudogap state observed in ultrathin titanium nitride (TiN) films [5], the authors claimed that the pseudogap arose from the suppression of DOS by quasi-2D superconducting fluctuations, even at temperatures higher than the transition temperature. Unfortunately, the latter three models cannot provide a mechanism for the pseudopeak observed in experiment.

To settle the debate, we have chosen three metals, i.e., lead (Pb), aluminum (Al), and indium (In), with different Debye energies and electron-phonon mass enhancement parameters. These two parameters play a critical role in Wang's model [1]. By growing them on a Si(111) surface with various island sizes, we have constantly observed the pseudogap state in all samples as long as the quantum confinement effect exists and the QWSs are away from the Fermi level. For Pb and Al islands of special thickness with a QWS at/near the Fermi level, the pseudopeak features were again observed. Our data clearly show that for very large islands the width of the pseudogap is directly proportional to the Debye energy, which provides direct evidence that the interplay between the quantum confinement and the electron-phonon scattering is an indisputable mechanism for the pseudogap state. As the island size becomes small, the dynamic Coulomb blockade effect starts to dominate as demonstrated by Brun *et al.* [3]; and with further island size decrease the normal Coulomb blockade effect eventually takes place. Therefore, our results have demonstrated that different mechanisms dominate the size and shape of the pseudogap state for different island size regimes.

II. EXPERIMENTS

Our experiments were performed in ultrahigh vacuum chambers with sample growth facilities and an Omicron low-temperature scanning tunneling microscope (STM), for which we have improved the control system to filter out rf noises and successfully improved its energy resolution from a level of 0.9 to a level of 0.2 meV [6].

The substrate used in our experiments was a highly doped *n*-type Si(111) wafer which was treated by a standard procedure to form a 7×7 surface reconstruction. In order to compare the pseudogap states in the In, Al, and Pb islands, it was preferable to prepare these islands with similar size and shape. By properly controlling the deposited quantity of Pb, the substrate temperature, and the annealing time at room temperature (RT), the Pb islands grown on Si(111) with a predeposited conductive Pb wetting layer could be well controlled to reach the desired size and thickness. Because there were no similar conductive wetting layers, the growth

*Corresponding author: wangkd@sustc.edu.cn
†xdxiao@phy.cuhk.edu.hk

of In and Al islands required a different approach to solve their conductance problem. For instance, when In islands were directly grown on the In wetting layer on a Si(111) surface, the scanning tunneling spectroscopy (STS) measurement within a narrow bias range near the Fermi level at low temperatures (4.2 K) could not be properly performed [7], in strong contrast to the case of Pb islands grown on a Pb wetting layer. To attack the conduction problem, we have taken the following two approaches and eventually successfully resolved this problem in both In and Al systems. In the first approach, we first grew a Pb wetting layer on the Si(111) surface, then grew the flat-top In or Al metallic islands on the Pb wetting layer. Because of the good conductivity of the Pb wetting layer, the conductance between the In islands and the external electrode could be well achieved via the Pb wetting layer and proper STS measurement could be well performed. Unfortunately this approach did not work for Al islands. We had to take the second approach to grow Al islands on the surface of a relatively thin Al film. By taking a two-step growth mode with an Al wetting layer deposited on Si(111) first at liquid nitrogen temperature and Al islands deposited at room temperature, the resultant Al sample consisted of flat-top Al islands on top of a monolayer thick Al wetting layer. Again, the conductance between the Al islands and the external electrode at low temperatures was established via the monolayer Al film.

After successfully preparing the flat-top Pb, In, and Al islands, we measured their electronic properties by STS with a W tip in a temperature range from ∼3.0 to ∼15 K. The *in situ* tracking of a given island at varied temperatures ensured the high reproducibility of the STS spectra, thus providing high confidence for processing the spectra. Prior to the first use, the W tip was cleaned by e-beam heating in an ultrahigh vacuum. During the measurements, the W tip was carefully protected to avoid touching the sample surface to eliminate tip contamination by the sample materials. The differential conductance spectra of dI/dV were acquired from a lock-in amplifier with a modulation frequency of 500–1000 Hz. With the improved performance of the STM, a small peak-to-peak modulation of 0.2 mV was sufficient to acquire good quality dI/dV data.

III. RESULTS AND DISCUSSIONS

A. Growth behavior of the flat-top metallic islands

The growth of Pb follows the Stranski–Krastanov (S-K) growth mode, namely, it first forms a wetting layer completely covering the surface and then starts to grow three-dimensional (3D) islands [8]. Unlike the normal S-K mode, these 3D Pb islands do not have the normal hill-like shapes but have flat tops. Such flat-top behavior is a resultant of quantum size effect, that is, the island thickness tends to take certain values leading to a lower DOS at the Fermi level [9]. In the experiment, the lateral size of the Pb islands is mainly determined by the substrate temperature while the height depends largely on the deposited quantity of Pb. Figure 1 shows examples of Pb islands on Si(111)-7 × 7 surface with Pb coverage of about 3.2 ML. Figures 1(a) and 1(c) demonstrate that the size and density of Pb islands strongly depend on the substrate temperature. The deposited Pb atoms aggregate into large volcano shaped islands with low density at 270 K but small flat-top islands with high density at 200 K. The volcano shaped islands [Fig. 1(a)] can evolve into flat-top islands [Fig. 1(b)] after annealing at RT for about 30 min.

As mentioned above, the In islands can grow on top of the Pb wetting layer and their growth behavior is similar to that of Pb islands. In our experiments we deposit about 1 ML Pb atoms onto the Si(111) surface to form the wetting layer. Subsequent STM imaging showed no additional Pb islands or clusters on this layer. On top of the Pb wetting layer, an appropriate amount of In atoms are deposited to grow In islands. Figure 2 shows that an In island grown at RT without further annealing has a flat top and is very similar to the Pb islands after RT annealing [Fig. 1(b)].

The growth of large Al islands is problematic. We have attempted several methods to prepare satisfactory Al islands samples. Both directly growing Al islands on Si(111)-7 × 7 surface at RT and indirectly growing Al islands on the predeposited Pb wetting layer fail to provide good conduction between the Al island and the external electrode. A conductive sample can finally be obtained when the Al islands are grown on a low-temperature predeposited Al wetting layer. Presumably a reaction between the Al wetting layer and

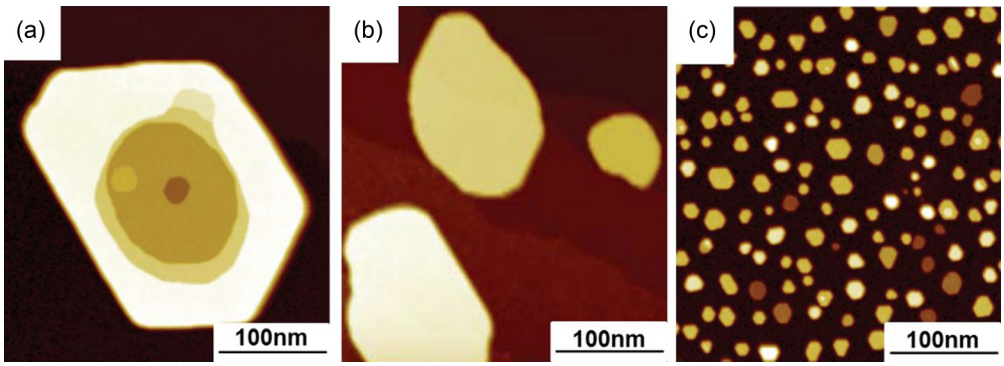

FIG. 1. (Color online) Pb islands grown at different temperatures with a Pb coverage of about 3.2 ML. The lateral size of the Pb islands decreases from ∼10 000 nm^2 with substrate temperature of 270 K (a) to ∼10 nm^2 with substrate temperature of 200 K (c). The volcano shaped islands grown at 270 K could change into flat-top ones (b) after annealing at RT for 30 min. The image size is 300 × 300 nm^2 and the imaging conditions are $V_{\text{sample}} = -2$ V and $I_t = 0.3$ nA.

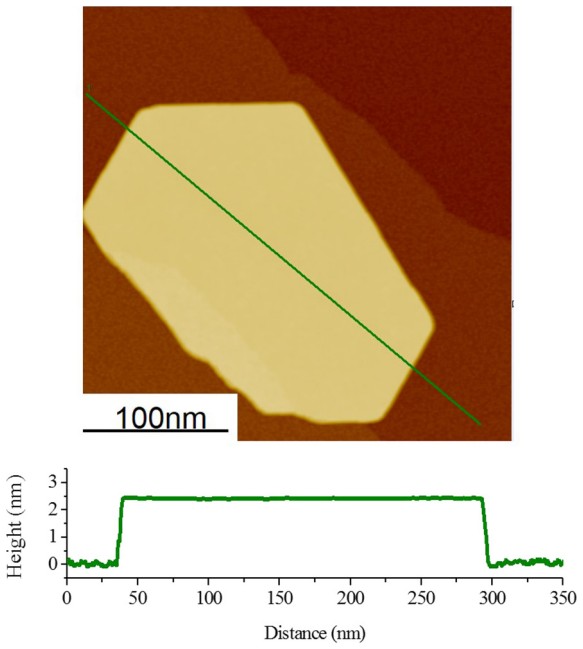

FIG. 2. (Color online) An In island grown on Pb wetting layer at RT. Image size is 300 × 300 nm^2 and the imaging conditions are $V_{\text{sample}} = -2$ V and $I_t = 0.3$ nA.

the Si substrate at the Al/Si interface takes place at RT to destroy the conductance of the Al wetting layer [10]. But this reaction can fortunately be largely suppressed in low-temperature growth to retain the conductivity of the Al wetting layer. In our case, the Al wetting layer on Si(111) is grown at 150 K by depositing about 1 ML Al on the substrate and the Al islands are grown at RT by depositing about 5.5 ML Al on top of the low-temperature grown Al wetting layer. An STM image in Fig. 3(a) demonstrates such Al islands grown on the Al wetting layer at RT. The irregularly shaped large Al islands often possess an edge-edge angle of 120°, indicating the (111) orientation of the islands and the possible mergence from small islands. Among the large islands, there are many small rectangular islands of (001) orientation, similar to those observed by reflection high-energy

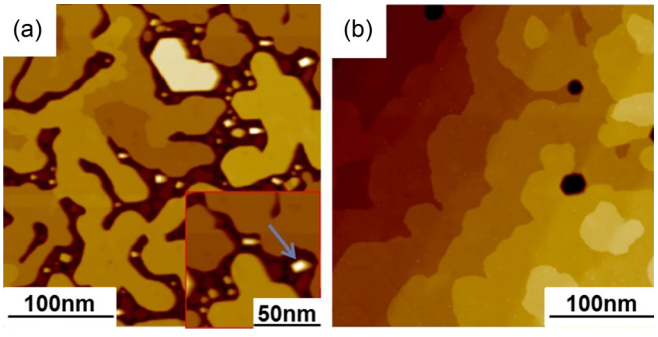

FIG. 3. (Color online) (a) Al islands grown at RT on an Al wetting layer prepared at 150 K. The inset shows the small islands of (001) orientation among the large islands. The image size is 300 × 300 nm^2 and the imaging conditions are $V_{\text{sample}} = -2$ V and $I_t = 0.3$ nA. (b) Al film with a thickness of ∼7 ML grown at 150 K.

electron diffraction (RHEED) in Ref. [11], which prevent further connection between large islands [shown in the inset of Fig. 3(a)]. In comparison, Fig. 3(b) shows an Al film grown on Si(111)-7 × 7 surface at 150 K with ∼7 ML thickness.

B. Quantum well states of metallic islands

As reported previously [12–18], quantum well states (QWSs) are readily observable in all the flat-top islands. Confinement by the island-substrate interface and the island-vacuum interface for electrons in these flat-top islands introduces interference as the Fabry-Pérot effect in optics and produces separated electronic states, namely, QWSs. The positions of the QWSs are determined by the Bohr-Sommerfeld quantization rule [19], $2k(E)Nt + \Phi(E) = 2n\pi$, where $k(E)$ is the electron wave vector, N is the number of metal monolayer, t is the monolayer thickness, and Φ is the boundary phase shift.

In Fig. 4 the differential conductance dI/dV curves illustrate the existence and the periodicity of QWSs in the three different kinds of islands, where peaks in the dI/dV curves clearly represent the energy positions of the QWSs. The DOS at the Fermi level is greatly influenced by the positions of the QWSs. Within a finite energy window around the Fermi level, the Bohr-Sommerfeld quantization rule implies that there is a thickness periodicity of $\Delta N = \frac{\lambda_F}{2t} = 2.2$ for Pb islands, i.e., nearly every two Pb layers there is a QWS peak to occur near the Fermi level [20]. Therefore, the DOS at the Fermi level oscillates with a period of ∼2 ML for Pb islands. Similarly, for the In and Al islands, the corresponding values are $\frac{\lambda_F}{2t} = 4\frac{\lambda_F/2}{d}$ [16] and $\frac{\lambda_F}{2t} = 0.77$ [17], respectively. Thus, the DOS at the Fermi level oscillates with different periods in thickness for the three different materials.

C. Superconductivity-pseudogap transition in Pb, In islands and pseudogap state evolution in Al islands

1. Pb and In islands

Figures 5(a) and 5(d) show the STM topographic images of selected flat-top large Pb and In islands of comparable size and thickness, respectively. The QWSs are clearly shown in their insets with the corresponding large energy scale differential conductance dI/dV spectra taken at the position marked "×".

The selected Pb island has an area of 57 000 nm^2 and a thickness of 9 ML in the lower part and a thickness of 8 ML in the upper part. The selected In island has an area of 40 600 nm^2 and a thickness from 9 to 13 ML sequentially from left to right. A number of high energy resolution differential conductance dI/dV spectra of these two islands taken at the marked "×" positions of 9 ML thickness have been measured in the temperature range from 3.3 to 15.0 K, as shown in Figs. 5(b) and 5(e). Since the nearby QWSs are far away from the Fermi level for the given thickness of the Pb and In islands, the dI/dV spectra in the small bias range, −20 to 20 mV, have very flat backgrounds. As shown in Figs. 5(b) and 5(e), in addition to the superconductivity gaps sandwiched between the two coherent condensate peaks in the dI/dV spectra appeared at lower temperatures, the shallow pseudogaps without coherent peaks around them are observed at higher temperatures, and become weaker and weaker as temperature further increases.

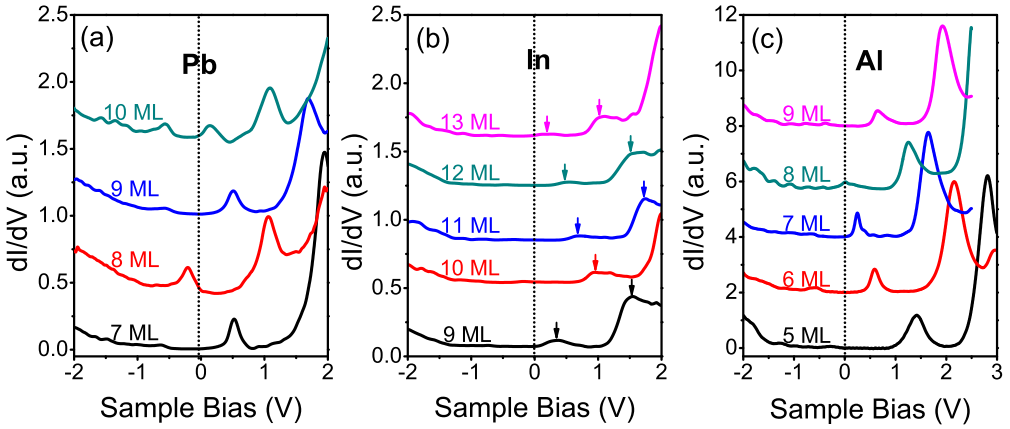

FIG. 4. (Color online) dI/dV curves demonstrating the QWSs of Pb, In, and Al islands with various thickness.

The evolution of the gap feature from 3.0 to 8.0 K is very similar for these two kind of metallic islands. In Figs. 5(c) and 5(f) the zero bias conductance (ZBC) clearly demonstrates the transition from the superconductivity state to the pseudogap state. At low temperatures, ZBC follows a power law behavior $ZBC = AT^p$, where parameters A and p are dependent on the materials and the size of the island. At relative high temperatures, ZBC shows a nearly linear relationship with temperature. The different behaviors of ZBC with temperature owe to the coexistence of superconductivity and pseudogap effects below the transition temperature (T_c) and pseudogap effect left alone above T_c. If we take the intersections of the two fitting lines of ZBC in the lower temperature region and higher temperature region as T_c, the transition temperature of superconductivity T_c is 6.64 K for the Pb island and 4.45 K for the In island, respectively. Such deduced transition temperature is lower than its bulk value for Pb (7.2 K) but higher than its bulk value for In (3.4 K), consistent with previous reports on size effects [6,21,22].

It is not surprising to find that the measured T_c of the islands has a noticeable deviation from the superconducting transition temperature of the corresponding bulk materials, decreased for Pb island but increased for In island.

For the In island, since the island is grown on a Pb wetting layer, the enhanced T_c can be attributed to two factors. First, the surface phonon softening effect arises due to the structural transformation in a nanosized In island [23]. Along with the phonon softening, the electron-phonon coupling strength increases and hence undermines the basis of BCS theory which is valid for bulk In. In the strong coupling limit, according to

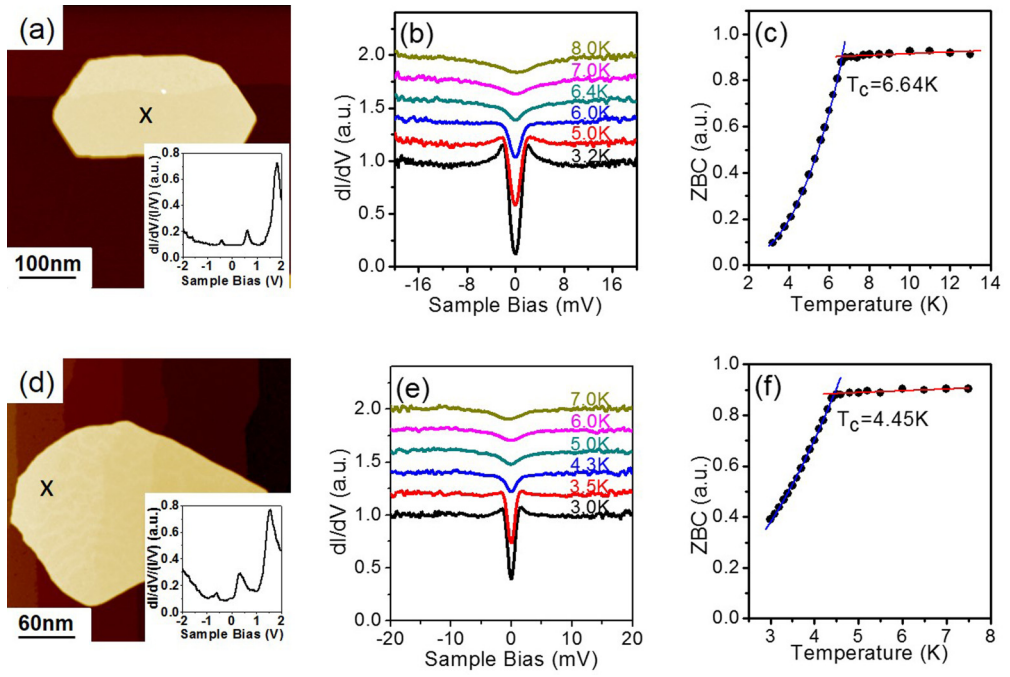

FIG. 5. (Color online) STM images of a large Pb island (a) and a large In island (d) of similar size. Inset: QWSs of 9 ML Pb island and 9 ML In island measured at the positions marked "×" in the figures. At the same positions, a set of selected differential conductance dI/dV spectra at various temperatures measured with setpoint $V_{\text{sample}} = -20$ mV and $I_t = 1$ nA are shown in (b) and (e), respectively, for Pb and In islands. The deduced ZBC data versus temperature for Pb island and In island are plotted in (c) and (f).

McMillan's equation [24], the transition temperature is given by

$$T_c = \frac{\Theta_D}{1.45} \exp\left[\frac{-1.04(1+\lambda)}{\lambda - \mu^*(1+0.62\lambda)}\right],$$

where Θ_D is the Debye temperature, μ^* is the Coulomb pseudopotential, and λ is the electron-phonon mass enhancement parameters. Here λ is roughly inversely proportional to $\langle\omega^2\rangle$ which is an average of the square of the phonon frequency. In a nanosized island with a surface-to-volume ratio much higher than that of bulk, the surface phonon softening effect prevails. This is because the surface atoms have fewer interatomic bonds, which gives rise to overall lower phonon frequencies. With the phonon softening, the resultant increased λ eventually leads to a higher T_c [23,25,26]. According to Ref. [22], the T_c of In thin films can exceed 4.3 K when the film thickness decreases to 2–4 nm, making our experimental result reasonable [the interlayer spacing of In (111) planes is 0.274 nm and a 9 ML In film is 2.466 nm thick]. Second, since the In island is grown on a Pb wetting layer, incorporation of Pb atoms into the In island can also increase T_c [27]. Based on the results in Ref. [27], T_c can increase to about 4.45 K if the Pb concentration is 10% in a bulk In sample.

To interpret the change of T_c occurring in the Pb island we need to take into consideration the fact that bulk Pb is already a strong electron-phonon coupling superconductor. As the size of the Pb island decreases, especially when the system size is reduced below certain characteristic lengths including the London penetration depth $\lambda_L(T)$ and the coherence length $\xi(T)$, the quantum size effect originated from the discrete nature of the electronic energy levels will surpass other effects, such as surface phonon softening effect and play a dominant role in the superconductivity transition, resulting in a lower transition temperature [26,28–30].

2. *Al islands*

The topography of Al islands is shown in Fig. 6(a). Although the Al islands are very close to each other and have very different shapes from the isolated Pb or In islands with regular polygonal shapes, possibly due to different diffusion behaviors, the Al islands can still be well regarded as the 1D quantum confinement system. The size of the connected island is estimated to be larger than that of Pb and In islands described above, although the exact area is hard to measure. Similar to the Pb and In islands with 9 ML thickness, the large energy range dI/dV spectrum of a 9 ML thick Al island is shown in Fig. 6(b) and shows no QWS near the Fermi level. Again, when zooming in the energy scale, the pseudogap states are observed for this large Al island, as depicted in Fig. 6(c). Unlike the Pb or In islands, no superconducting transition is observed in the temperature range from 4.2 K and above, possibly because that the T_c of Al bulk is 1.2 K and any size effect for Al island cannot move the T_c into our accessed temperature range. More importantly, in contrast to the pseudogap states observed for Pb and In islands, the pseudogap for a large Al island appears shallower but with a much wider width [see Fig. 6(c)]. As will be discussed later, such pseudogap features support the model based on the interplay between the quantum confinement and the electron-phonon scattering.

3. *Various manifestation of the pseudogap state*

The above pseudogap states were observed in metallic islands with no QWS at/near the Fermi level. With the system energy minimized, islands with no QWS at Fermi level are very stable and are frequently observed. Nevertheless, metastable islands with a QWS at/near the Fermi level still exist. In Fig. 4(c) we notice from the dI/dV spectra that a QWS sits very close to the Fermi level for the 8 ML thick Al island. Similar to what has been reported for Pb islands at 18 and 27 ML thickness [1], instead of a pseudogap feature, a bump feature, or pseudopeak state, in the dI/dV curve emerges for the 8 ML thick Al island as well, as shown in Fig. 7(a). In Figs. 8(a) and 8(b) we show another example of pseudopeak state for the 18 ML thick Pb island. The intensity and width of these pseudopeaks are comparable to those of the pseudogap in a 9 ML thick Al island and a 9 ML thick Pb island, strongly implying that the pseudogap and pseudopeak feature must have the same origin.

Because the QWS position is sensitive to the island/semiconductor interface through the phase shift, the pseudopeak may appear either on the right or left side of QWS peak maximum [Figs. 8(a) and 8(b)], and sometimes may not even show up if the QWS peak maximum is sufficiently

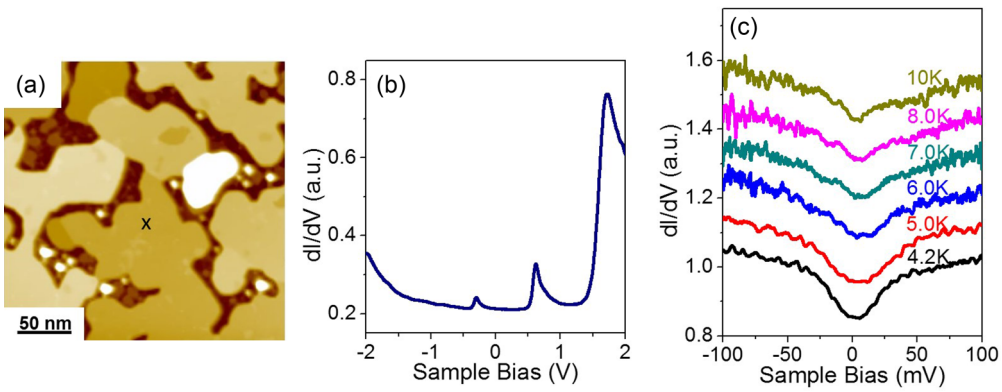

FIG. 6. (Color online) Pseudogap state in Al island. (a) STM image of connected Al islands. (b) QWSs of a 9 ML Al island, measured at the setpoint $V_{\text{sample}} = -2$ V and $I_t = 1$ nA. (c) dI/dV spectra of the Al island around the Fermi level at various temperatures. The setpoint for these dI/dV spectra is $V_{\text{sample}} = -100$ mV and $I_t = 1$ nA.

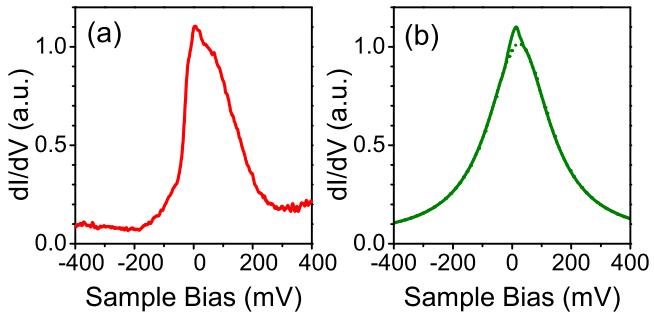

FIG. 7. (Color online) Pseudopeak state in 8 ML thick Al island. (a) dI/dV spectrum of the 8 ML Al island around the Fermi level. The setpoint for this dI/dV spectra is $V_{\text{sample}} = -1$ V and $I_t = 0.3$ nA. (b) Simulated dI/dV spectrum with electron-phonon scattering model which shows the pseudopeak feature (solid line). Without the electron-phonon scattering effect, the dI/dV peak is shown in the dashed line.

away from the Fermi level. In Fig. 9(a), for an 8 ML Pb island, the QWS position near the Fermi level shows up a larger variation due to variation of the phase shift. It again demonstrates in Fig. 9(b) that the pseudopeak is sensitive to the position of QWS with respect to the Fermi level: the pseudopeak emerges when the QWS is very close to the Fermi level and transforms into a pseudogap when the QWS is far away from the Fermi level. Thus, the pseudopeak state is not as robust as the pseudogap state, and requires careful search even on 8 ML Al islands or 18 ML Pb islands.

Figure 8(e) clearly demonstrates that the pseudopeak state, just as the pseudogap state, can coexist with superconductivity below the superconducting transition temperature. As the temperature rises, the superconductivity of Pb islands fades away as expected while the pseudopeak persists at relatively high temperature. The relationship between pseudogap (pseudopeak) and superconductivity in such conventional superconductors is still an open question at the current stage. In Schackert's work [2], neither the superconductivity nor the

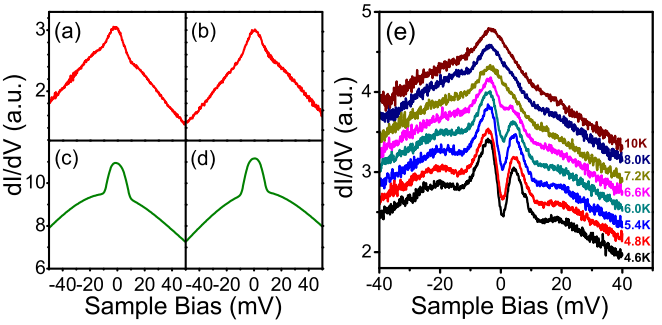

FIG. 8. (Color online) Pseudopeak states in 18 ML thick Pb island. (a) and (b) dI/dV spectra around the Fermi level measured at different positions on an 18 ML Pb island. The setpoint for these dI/dV spectra is $V_{\text{sample}} = -100$ mV and $I_t = 1$ nA. (c) and (d) Simulated dI/dV spectra with electron-phonon scattering model. (e) dI/dV spectra at various temperatures showing the evolution of superconductivity and pseudopeak for this Pb island. The superconductivity feature has been broadened by the instrument.

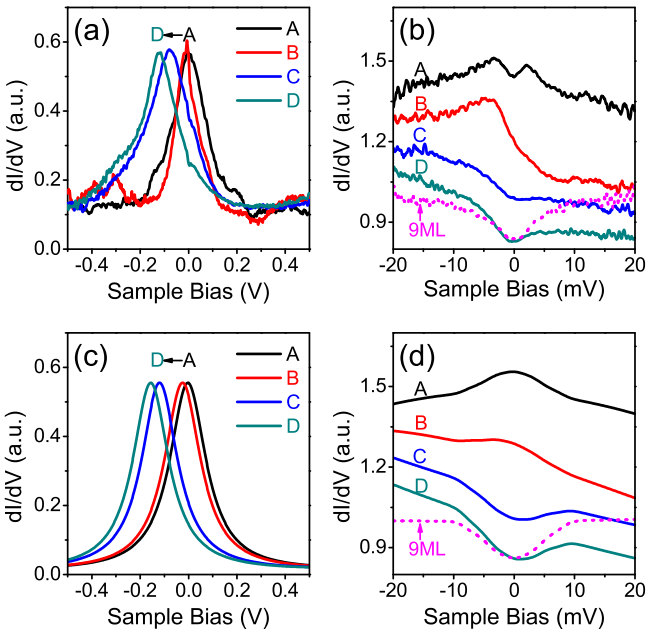

FIG. 9. (Color online) Transition from pseudopeak states to pseudogap states. (a) QWS near the Fermi level measured at different positions on an 8 ML Pb island at 8 K. The setpoint $V_{\text{sample}} = -2$ V and $I_t = 1$ nA. (b) Pseudogap or pseudopeak state on this 8 ML Pb island with slightly different QWS positions. The setpoint $V_{\text{sample}} = -20$ mV and $I_t = 1$ nA. The dashed line is the dI/dV curve measured on a 9 ML Pb island for reference. (c) The simulated QWS at different energy positions induced by changes in the phase shift. (d) The simulated pseudogap and pseudopeak features.

pseudopeak states were found in the 18 or 27 ML Pb islands grown on Cu(111).

Beside the pseudopeak observed above for islands with a QWS at/near the Fermi level, there are a number of other manifestations of the pseudogap state. For Pb and In islands with a given thickness, the width and depth of the pseudogap increases as the lateral size decreases, indicating a strong island size dependence, as depicted in Fig. 10(b) for the Pb islands shown in Fig. 10(a). For Al islands, the shape of the differential conductance dI/dV curves changes significantly with the decrease of Al island size. As shown in Fig. 11(a), a clear and wide pseudogap state with an inclined background originated from the nearby QWS of the 7 ML connected Al island can be well observed in the dI/dV curve. With a smaller Al island, the pseudogap state becomes much narrower and deeper, as shown in Fig. 11(b). Interestingly, when the size of the Al island is reduced down to $\sim$100 nm^2, a series of equal spaced peaks and a complete gap emerge in the differential conductance curve [see Fig. 11(c)], similar to what have been observed in the system of metallic islands grown on insulating layer covered substrates [3,31]. All these different manifestations of the pseudogap state must be properly understood and will be discussed in the next section.

D. Mechanisms of pseudogap state

Our observed pseudogap state may have different origins in different size regimes. Depending on the lateral length

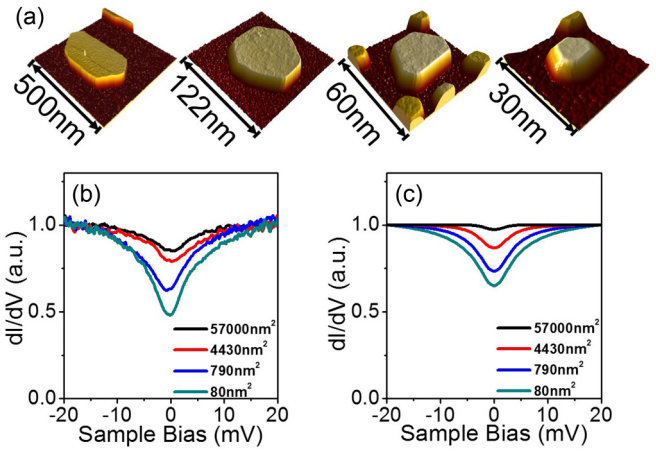

FIG. 10. (Color online) (a) STM images of a number of Pb islands of different sizes. (b) dI/dV spectra of 9 ML Pb islands with different lateral sizes measured at 8 K. All the spectra are measured at the setpoint of $V_{\text{sample}} = -20$ mV and $I_t = 1$ nA. (c) Calculated differential conductance dI/dV spectra of 9 ML Pb islands with DCB model.

scale of the islands, we will explain our observations based on semiquantitative analysis of the width and depth of the pseudogap: when the island size is very large, the interplay between the quantum confinement and the electron-phonon scattering is found to be the dominant mechanism for the pseudogap state; as the island lateral size decreases, the dynamic Coulomb blockade effect starts to take over; and with further island size decrease the orthodox Coulomb blockade effect eventually becomes important.

1. *Effect of electron-phonon scattering*

In the first model, the lateral size of the island is assumed to be irrelevant and the effect only depends on the island thickness. Physically, the DOS of thin metallic film can be described as a Fabry-Pérot spectral function [32]

$$\rho = \frac{1}{1 + \frac{4f^2}{\pi^2}\sin^2(kNt + \Phi/2)}, \tag{1}$$

where k is the electron wave vector, N is the number of metal monolayer, t is the monolayer thickness, Φ is the boundary phase shift, and f is the interferometer finesse given by

$$f = \frac{\pi R^{1/2} - \exp\left[Nt/l(\Gamma)\right]}{1 - R\exp\left[Nt/l(\Gamma)\right]}, \tag{2}$$

where R is the product of the reflectivity at the surface and the metal/semiconductor interface, and l is the coherence length or the mean free path of the quasiparticle. The quasiparticle mean free path l is determined by the quasiparticle lifetime $1/\Gamma$ and the group velocity υ as $l(\Gamma) = \upsilon/\Gamma$. Equation (1) yields a set of QWS peaks at the energy positions where the Bohr-Sommerfeld quantization rule [19,33,34] $2k(E)Nt + \Phi(E) = 2n\pi$ is satisfied. Considering the electron-phonon scattering as the major mechanism to affect the electron's lifetime, the interferometer finesse f becomes energy dependent and will open up a dip (peak), namely pseudogap (pseudopeak), for DOS at the Fermi level. Within the Debye approximation, the electron-phonon scattering rate Γ is given by [1,35,36]

$$\Gamma_{\text{e-ph}}(E,T) = 2\pi\int_0^{E_D}\lambda\left(\frac{E'}{E_D}\right)^2\left[1 - \frac{1}{\exp\left(\frac{E-E'}{k_BT}\right)+1} + \frac{1}{\exp\left(\frac{E+E'}{k_BT}\right)+1} + \frac{2}{\exp\left(\frac{E'}{k_BT}\right)+1}\right]dE', \tag{3}$$

where E_D is the Debye energy and λ is the electron-phonon mass enhancement parameter.

According to this model, the pseudogap can be influenced by a number of factors. Besides the temperature and thickness of the metallic film, E_D would determine the width of the pseudogap and λ and R would determine the depth of the pseudogap. Thus, the width and depth of the pseudogap of different materials are very important evidence to check the validity of this model.

To obtain the width and depth of the pseudogap for the very large islands, we use a Gaussian function to fit the dI/dV spectra at various temperatures after removing a temperature-independent background. As presented in Ref. [21], the width and depth have a linear relation with temperature. For the

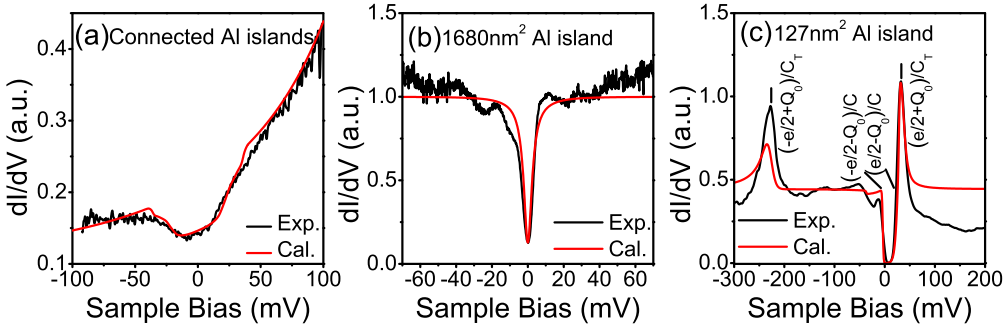

FIG. 11. (Color online) (a)–(c) dI/dV spectra of Al islands with different lateral sizes measured at 4.5 K together with simulated results with different models which are presented in the text. First two spectra are measured at the setpoint of $V_{\text{sample}} = -20$ mV and $I_t = 1$ nA, the third spectrum is taken at the setpoint of $V_{\text{sample}} = 2$ V and $I_t = 1$ nA. Values of parameters used in the calculation are as follows: (a) reflectivity of interface $R = 0.6$, phase shift $\Phi = 0.55\pi$; (b) $R = 0.11R_K, C = 15aF$, where R_K, the resistance quantum, is given by $R_K = h/e^2 = 25.8K\Omega$; (c) $R_T = 2G\Omega$, $R = 25M\Omega, C_T = 0.617aF, C = 4.9aF, Q_0 = -0.380e$.

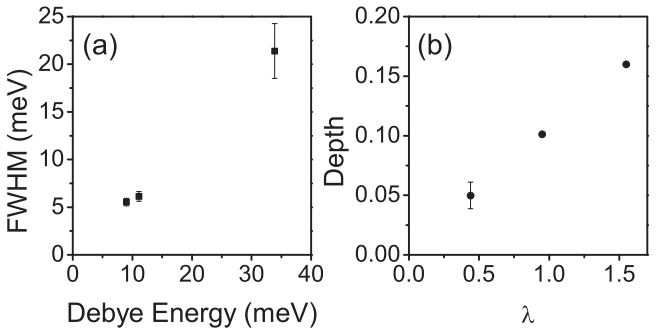

FIG. 12. Comparison of the width (a) and the depth (b) of pseudogap of islands formed by different materials at 8 K. The Debye energies are taken from Ref. [37] and $\lambda = 1.55$ for Pb, $\lambda = 0.95$ for In, and $\lambda = 0.44$ for Al are taken from Refs. [36,38,39] for the respective bulk materials.

comparison among three different kind metal islands, we use the fitted values of the width and depth at the same temperature, namely, 8.0 K from the largest Pb, In, and Al islands of 9 ML thick. Figure 12(a) shows the result of the full width at half maximum (FWHM) of the pseudogap as a function of the Debye energy and Fig. 12(b) shows the result of the depth of the pseudogap as a function of the electron-phonon mass enhancement parameter λ. As clearly shown, the width of the pseudogap has a nearly linear dependence on the Debye energy, with the widest pseudogap observed for Al due to its largest Debye energy; and the depth of the pseudogap depends linearly on λ, with the shallowest pseudogap observed for Al due to its smallest λ. Both features demonstrate semiquantitative agreement with Eq. (3), implying the decisive role of the electron-phonon scattering for the formation of the pseudogap state.

We have used Eqs. (1)–(3) to simulate the pseudogaps for the three large metallic islands. By taking E_D and λ from the bulk values, the electron reflectivity (R) and the phase shift (Φ) are used as fitting parameters. In order to fit the overall background for the large energy scale dI/dV curves, an energy independent scattering rate due to impurity scattering and a scattering rate term proportional to E^2 due to electron-electron scattering are also added in the simulation.

First of all, in addition to the thickness and the wave vector, the exact position of QWS is determined by the phase shift Φ which can be adjusted so that the calculated results can best fit the experimental data. Second, the electron reflectivity R affects the peak height of QWSs and the depth of pseudogap. In our fitting, this parameter is taken with similar values in all three islands ($R = 0.64$, 0.64, 0.58, respectively). As shown in Fig. 13, the pseudogap feature can be reasonably simulated with the Debye phonon spectrum, as denoted by red lines, with good agreement in the depth but somewhat fatter gaps than the observation. To understand the deviation between the experimental and calculated pseudogaps, we realize that the Debye phonon spectra cannot realistically represent the phonon spectrum of the materials. If we use the experimentally determined Eliashberg function of the respective bulk materials [40,41] instead of the Debye spectra, a better agreement can be obtained for Pb but a wider dip is simulated for an In island [Figs. 13(a) and 13(b) blue lines]. For the Al island, no obvious improvement on the simulation was found except a sunken feature at the edge of the dip. While it is reasonable to speculate that the island Eliashberg function can differ from that of the bulk, as confirmed by Refs. [42,43], the simulated pseudogap result with the available Eliashberg function for 13 ML Pb island [2] indeed agrees with the experiment even better, as shown by a green line in Fig. 13(a). Considering other unknown factors including the actual phonon spectrum of the specific metallic islands and the instrumental convolution in the experiment, the origin of the somewhat larger gaps for large Pb, In, and Al islands is semiquantitatively confirmed as due to the interplay between the quantum confinement and the electron-phonon scattering.

The further support of this mechanism comes from the pseudopeak features observed in our experiment (Sec. III C) and simulated by Eqs. (1)–(3) when there is a QWS at/near the Fermi level. The models discussed later cannot provide an explanation to the pseudopeak feature and therefore cannot reject the important role played by the electron-phonon scattering in these flat-top islands with quantum confinement. As shown in Figs. 7(b), 8(c), 8(d), 9(c), and 9(d), the simulated pseudopeak features based on Eqs. (1)–(3) describe convincingly the experimental observations. Even more strikingly, the position sensitivity of the pseudopeak state to the position variation of the QWS near the Fermi level is built in the present model. As demonstrated in Fig. 9, the observed shift of QWS near the Fermi level and the transition from pseudopeak states to pseudogap states can be well reproduced in our simulation, simply by employing an adjustable phase shift Φ.

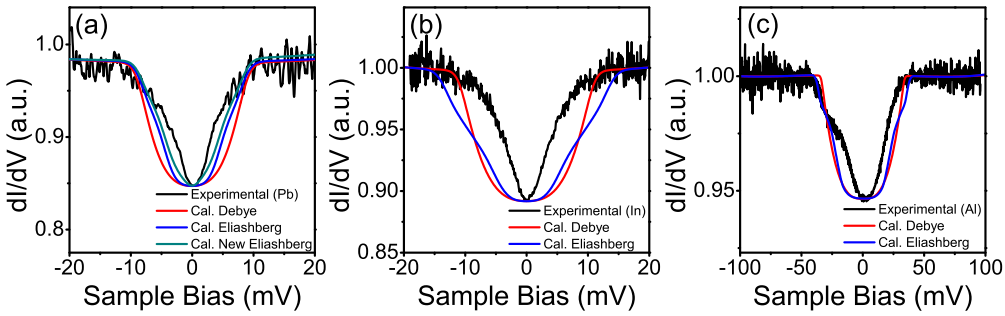

FIG. 13. (Color online) Comparison between experimental pseudogap and simulated pseudogap by Eqs. (1)–(3). (a) For Pb, with simulations employed different phonon spectra. (b) For In, with simulations employed different phonon spectra. (c) For Al, with simulations employed different phonon spectra.

2. Effect of dynamic Coulomb blockade

The shortcoming of the above model based on the interplay between the quantum confinement and the electron-phonon scattering is that there is no explicit consideration in the lateral size of the metallic island. This is of course deviating from the experimental observations. In order to understand the size dependence, Brun *et al.* proposed a different model. By considering the metal-semiconductor contact with a finite capacitance and resistance, they formulated a dynamic Coulomb blockade (DCB) model [3,44].

In the DCB model, four parameters, which are the resistance (R_T) and capacitance (C_T) of the tunnel junction and the resistance (R) and capacitance (C) of the interface between the island and substrate, are employed to describe the tunneling current through the junction at a given sample bias. The tunneling current is $I = e[\Gamma(eV) - \Gamma(-eV)]$ and the tunneling rate can be expressed in the form of convolution product [44,45]

$$\Gamma(eV) = \frac{1}{e^2 R_T}\int_{-\infty}^{+\infty}\gamma(\varepsilon)P(\varepsilon - eV)d\varepsilon = \frac{1}{e^2 R_T}\gamma * P(eV), \tag{4}$$

where

$$\gamma(E) = E/(1 - e^{-E/k_BT}) \quad \text{and}$$
$$P(E) = \frac{1}{2\pi\hbar}\int_{-\infty}^{+\infty}\exp\left[J(t) + \frac{iEt}{\hbar}\right]dt. \tag{5}$$

The quantities $\gamma(E)/e^2R_T$ and $P(E)$, respectively, represent, during the tunneling process, the probability that an electron emits an energy E to the electromagnetic environment and the probability that the electromagnetic environment absorbs an energy E. The phase correlation function $J(t)$ can be obtained by the quantum fluctuation dissipation theorem:

$$J(t) = 2\int_{-\infty}^{+\infty}\frac{\mathrm{Re}Z(\omega)}{R_K}\frac{e^{-i\omega t} - 1}{1 - e^{-\hbar\omega/k_BT}}\frac{d\omega}{\omega}, \tag{6}$$

where the resistive part of total impedance $Z(\omega)$ is involved and the total impedance can be expressed as $Z(\omega) = [i\omega(C + C_T) + R^{-1} + {R_T}^{-1}]^{-1}$. Normally the resistance of tunnel junction R_T is much larger than that between islands and substrates. As such, we can neglect the term of ${R_T}^{-1}$ and then the total impedance can be written as $Z(\omega) = [i\omega C + C_T + R^{-1}]^{-1}$.

With Eqs. (4)–(6) above, we can calculate the differential conductance dI/dV spectra for the Pb islands of different sizes. As shown in Fig. 10(c), the DCB model can explain the size effect of the pseudogap [Fig. 10(b)] since the width of the blockade dip is directly related to the capacitance and hence the area of the island. Here the fitting parameters of resistance (R) and capacitance (C) are obtained from the empirical formula which shows roughly a liner relationship between the capacitance (resistance) and the area of islands (the inverse area of the islands) as in Ref. [3].

While this model has a built-in island size dependence and can quantitatively explain the pseudogap in small islands, the fitting quality to the dI/dV curves taken on Pb samples showed strong deviations for large islands even in Ref. [3]. As demonstrated in Fig. 10(c), the DCB model would practically simulate no pseudogap state for the largest island in our experiment, showing quantitative disagreement. Therefore, we must conclude that the observed pseudogaps in islands with different sizes have different dominant mechanisms. Coexistence of the above two mechanisms is essential to reach a comprehensive understanding of all the observed pseudogap features.

The coexistence of the above two mechanisms may directly come from the data in Fig. 9(b). Superimposed on the pseudopeak state of point A is an unexpected small dip (at 8 K). The possible explanation is that the dynamical Coulomb blockade effect sets in while the pseudopeak is established on top of the QWS peak.

3. Effect of orthodox Coulomb blockade

As shown in Fig. 11(c), for an Al island of size ~100 nm^2, a series of equal spaced peaks and a complete gap emerge in the differential conductance dI/dV curve. In contrast, Pb and In islands with comparable size do not shown such behavior; only a single pseudogap feature is observed at the Fermi level.

The remaining question is why the Al/Si interface tends to serve as the insulating layer instead of the well conducting wetting layer, especially for Al islands of small size. The answer would be that the reaction at the Al/Si interface, as mentioned above, may produce a highly resistive layer and can thus block the electrons from flowing to the substrate to some extent [10]. Even with our procedure of first preparing an Al wetting layer about 1 ML at low temperature and then growing the Al islands at ambient temperature to greatly suppress the reaction between Al and Si, the resistance of the interface is still non-negligible, in particular for small Al islands for which the resistance is inversely proportional to the island area. With a significant resistance in the metal/semiconductor contact, a Coulomb blockade effect can occur for the small Al islands.

As shown in Fig. 11(c), we employed the orthodox theory of Coulomb blockade to simulate the dI/dV spectra obtained on the small-sized Al island. Our system, consisting of the tip, vacuum junction, metallic islands, and the substrate, forms two mesoscopic tunnel junctions coupled in series and can be characterized by five parameters, among which four of them are the same as those used in the DCB model: the resistance (R_T) and capacitance (C_T) of the tunnel junction and the resistance (R) and capacitance (C) of the interface between the island and substrate, and the fifth being the residual charge in the islands Q_0 which can lead to an asymmetric dI/dV spectrum. Unlike DCB effect, comparing to R_T, R is no longer negligible now. With the detailed formulation given in Refs. [46,47], we can simulate the experimental dI/dV spectrum in Fig. 11(c) by a set of parameters given in the figure caption. Clearly the orthodox Coulomb blockade effect can well explain the observed equally spaced peaks and the complete gap in the dI/dV curve for the ~100 nm^2 Al island.

IV. CONCLUSION

In summary, we have demonstrated that the pseudogap exists in all the metallic islands made of Pb, In, and Al when the metal-substrate interface has a good conductivity. Through comparing the width and depth of the pseudogaps in very large Pb, In, and Al islands, we revealed that the width of

the pseudogap is strongly dependent on the Debye energy and the depth of the pseudogap is linearly related to the electron-phonon mass enhancement parameter. This result has provided direct evidence that the pseudogap state is semiquantitatively consistent with the model based on the interplay between the quantum confinement and the electron-phonon scattering for electrons in a two-dimensional thin film. Observations of pseudopeaks in Pb and Al islands with a QWS near their Fermi levels have further lent support to this model since only the interplay between the quantum confinement and the electron-phonon scattering can induce such a manifestation.

DCB effect has been invoked to semiquantitatively explain the observed evolution of pseudogap as the island size continuously decreases. To attribute the pseudogap state as entirely due to DCB effect would fail quantitatively for large sized islands. We have therefore reached a conclusion that the electron-phonon scattering effect and the DCB effect coexist and become the dominant mechanism for the formation of pseudogap (pseudopeak) state in different island size regimes. The interplay between electron-phonon scattering and the quantum confinement is mainly responsible for the formation of the pseudogap state in large metallic islands, while the DCB effect dominates the pseudogap state in small metallic islands. In some special cases, our experimental results directly demonstrate these two effects coexist. Our systematic study on such pseudogap (pseudopeak) state should have provided a comprehensive understanding on these phenomena and settled previous debates on the mechanisms.

ACKNOWLEDGMENT

This work was supported by the Research Grants Council of Hong Kong (Grants No. 404613 and No. 403311).

[1] K. D. Wang, X. Q. Zhang, M. M. Loy, T.-C. Chiang, and X. D. Xiao, Phys. Rev. Lett. **102**, 076801 (2009).
[2] M. Schackert, T. Markl, J. Jandke, M. Holzer, S. Ostanin, E. K. U. Gross, A. Ernst, and W. Wulfhekel, Phys. Rev. Lett. **114**, 047002 (2015).
[3] C. Brun, K. H. Müller, I.-Po Hong, F. Patthey, C. Flindt, and W.-D. Schneider, Phys. Rev. Lett. **108**, 126802 (2012).
[4] J. Kim, G. A. Fiete, H. Nam, A. H. MacDonald, and C. K. Shih, Phys. Rev. B **84**, 014517 (2011).
[5] B. Sacepe, C. Chapelier, T. I. Baturina, V. M. Vinokur, M. R. Baklanov, and M. Sanquer, Nat. Commun. **1**, 140 (2010).
[6] J. P. Liu, X. F. Wu, F. F. Ming, K. D. Wang, and X. D. Xiao, Supercond. Sci. Technol. **26**, 085009 (2013).
[7] K. D. Wang, X. Q. Zhang, M. M. T. Loy, and X. D. Xiao, Surf. Sci. **602**, 1217 (2008).
[8] H. H. Weitering, D. R. Heslinga, and T. Hibma, Phys. Rev. B **45**, 5991 (1992).
[9] S. C. Li, X. C. Ma, J. F. Jia, Y. F. Zhang, D. M. Chen, Q. Niu, F. Liu, P. S. Weiss, and Q. K. Xue, Phys. Rev. B **74**, 075410 (2006).
[10] H. J. Wen, M. Dähne-Prietsch, A. Bauer, M. T. Cuberes, I. Manke, and G. Kaindl, J. Vac. Sci. Technol. A **13**, 2399 (1995).
[11] H. Liu, Y. F. Zhang, D. Y. Wang, M. H. Pan, J. F. Jia, and Q. K. Xue, Surf. Sci. **571**, 5 (2004).
[12] F. Patthey and W.-D. Schneider, Phys. Rev. B **50**, 17560 (1994).
[13] D. A. Evans, M. Alonso, R. Cimino, and K. Horn, Phys. Rev. Lett. **70**, 3483 (1993).
[14] M. C. Yang, C. L. Lin, W. B. Su, S. P. Lin, S. M. Lu, H. Y. Lin, C. S. Chang, W. K. Hsu, and T. T. Tsong, Phys. Rev. Lett. **102**, 196102 (2009).
[15] W. B. Su, S. H. Chang, W. B. Jian, C. S. Chang, L. J. Chen, and T. T. Tsong, Phys. Rev. Lett. **86**, 5116 (2001).
[16] I. B. Altfeder, X. Liang, T. Yamada, D. M. Chen, and V. Narayanamurti, Phys. Rev. Lett. **92**, 226404 (2004).
[17] Y. Jiang, K. Wu, Z. Tang, P. Ebert, and E. G. Wang, Phys. Rev. B **76**, 035409 (2007).
[18] I.-Po Hong, C. Brun, F. Patthey, I. Yu. Sklyadneva, X. Zubizarreta, R. Heid, V. M. Silkin, P. M. Echenique, K. P. Bohnen, E. V. Chulkov, and W.-D. Schneider, Phys. Rev. B **80**, 081409(R) (2009).
[19] T.-C. Chiang, Surf. Sci. Rep. **39**, 181 (2000).
[20] C. M. Wei and M. Y. Chou, Phys. Rev. B **66**, 233408 (2002).
[21] J. P. Liu, X. F. Wu, F. F. Ming, X. Q. Zhang, K. D. Wang, B. Wang, and X. D. Xiao, J. Phys. Condens. Matter **23**, 265007 (2011).
[22] A. M. Toxen, Phys. Rev. **123**, 442 (1961).
[23] W. H. Li, C. C. Yang, F. C. Tsao, S. Y. Wu, P. J. Huang, M. K. Chung, and Y. D. Yao, Phys. Rev. B **72**, 214516 (2005).
[24] W. L. McMillan, Phys. Rev. **167**, 331 (1968).
[25] J. Dickey and A. Paskin, Phys. Rev. Lett. **21**, 1441 (1968).
[26] S. Bose, C. Galande, S. P. Chockalingam, R. Banerjee, P. Raychaudhuri, and P. Ayyub, J. Phys. Condens. Matter **21**, 205702 (2009).
[27] M. F. Merriam, Phys. Rev. Lett. **11**, 321 (1963).
[28] W. H. Li, C. C. Yang, F. C. Tsao, and K. C. Lee, Phys. Rev. B **68**, 184507 (2003).
[29] C. Brun, I.-Po Hong, F. Patthey, I. Yu. Sklyadneva, R. Heid, P. M. Echenique, K. P. Bohnen, E. V. Chulkov, and W.-D. Schneider, Phys. Rev. Lett. **102**, 207002 (2009).
[30] D. Eom, S. Qin, M. Y. Chou, and C. K. Shih, Phys. Rev. Lett. **96**, 027005 (2006).
[31] I. P. Hong, C. Brun, M. Pivetta, F. Patthey, and W.-D. Schneider, Front. Phys. **1**, 13 (2013).
[32] J. J. Paggel, T. Miller, and T.-C. Chiang, Science **283**, 1709 (1999).
[33] M. Milun, P. Pervan, and D. P. Woodruff, Rep. Prog. Phy. **65**, 99 (2002).
[34] D. A. Ricci, T. Miller, and T. C. Chiang, Phys. Rev. Lett. **93**, 136801 (2004).
[35] B. A. McDougall, T. Balasubramanian, and E. Jensen, Phys. Rev. B **51**, 13891 (1995).
[36] G. Grimvall, *The Electron-Phonon Interaction in Metals* (North-Holland, Amsterdam, 1981), Vols. 8 and 9.
[37] R. W. Powell and Y. S. Touloukian, Science **181**, 999 (1973).
[38] R. J. Higgins, H. D. Kaehn, and J. H. Condon, Phys. Rev. **181**, 1059 (1969).
[39] S. Y. Savrasov, D. Y. Savrasov, and O. K. Andersen, Phys. Rev. Lett. **72**, 372 (1994).
[40] J. Noffsinger and M. L. Cohen, Phys. Rev. B **81**, 214519 (2010).

[41] S. P. Rudin, R. Bauer, A. Y. Liu, and J. K. Freericks, Phys. Rev. B **58**, 14511 (1998).
[42] Y. F. Zhu, J. S. Lian, and Q. Jiang, J. Phys. Chem. C **113**, 16896 (2009).
[43] M. Dippel, A. Maier, V. Gimple, H. Wider, W. E. Evenson, R. L. Rasera, and G. Schatz, Phys. Rev. Lett. **87**, 095505 (2001).
[44] P. Joyez and D. Esteve, Phys. Rev. B **56**, 1848 (1997).
[45] A. A. Odintsov, G. Falci, and G. Schön, Phys. Rev. B **44**, 13089 (1991).
[46] M. Amman, R. Wilkins, E. Ben-Jacob, P. D. Maker, and R. C. Jaklevic, Phys. Rev. B **43**, 1146 (1991).
[47] A. E. Hanna and M. Tinkham, Phys. Rev. B **44**, 5919 (1991).